

Dynamical Evolution of Barred Galaxies

E. Athanassoula

Observatoire de Marseille, 2 Place Le Verrier, 13248 Marseille Cédex 04, France

August, 2004

Abstract. Angular momentum redistribution within barred galaxies drives their dynamical evolution. Angular momentum is emitted mainly by near-resonant material in the bar region and absorbed by resonant material mainly in the outer disc and in the halo. This exchange determines the strength of the bar, the decrease of its pattern speed, as well as its morphology. If the galaxy has also a gaseous component and/or a companion or satellite, then these also take part in the angular momentum exchange. During the evolution a bar structure forms in the inner parts of the halo as well. This bar is shorter and fatter than the disc bar and stays so all through the simulation, although its length grows considerably with time. Viewed edge-on, the bar in the disc component acquires a boxy or peanut shape. I describe the families of periodic orbits that explain such structures and review the observations showing that boxy/peanut ‘bulges’ are in fact just bars seen edge-on.

Keywords: barred galaxies, dynamical evolution, halo, peanuts, bulges

1. Introduction

Bars are very common features in disc galaxies. Eskridge et al. (2000), using a statistically well-defined sample of 186 disc galaxies from the Ohio State University Bright Spiral Galaxy Survey, find that 56% are strongly barred in the H band, while another 16% are weakly barred. Grosbøl et al. (2002), using a smaller sample of 53 spirals observed in the K band, find that about 75% of them have bars or ovals. These bars can have very different morphologies, from short to long, and from fat to thin, or from rectangular-like to elliptical-like. Thus we need to explain not only their formation, but also the distribution of their parameters and their different morphologies.

The spontaneous formation of bars in galactic discs was already shown in N -body simulations of the early seventies (e.g. Miller et al. 1970, Hohl 1971). At that time, the observational evidence for the existence of dark haloes around individual galaxies was hardly compelling, so the discs in these simulations were self-gravitating. Only a few years later haloes were propelled into the center of scientific discussions. Ostriker and Peebles (1973) were the first to check the effect of a heavy halo on the bar instability and found it to be stabilising. Although the number of particles in their simulations did not exceed 500, their work is very insightful. They introduced the parameter t_{op} , which is the



© 2019 Kluwer Academic Publishers. Printed in the Netherlands.

ratio of kinetic energy of rotation to total gravitational energy. They concluded that halo-to-disc mass ratios of 1 to 2.5 and an initial value of $t_{op} = 0.14 \pm 0.03$ are required for stability. Several later papers (e.g. Athanassoula and Sellwood 1986) confirmed the stabilising tendency of the halo. Yet, as we will see in the next section, this is an artifact, due to the fact that these simulations were either 2D, or had a rigid halo, or had too few particles. Thus the halo was not properly described. Before I discuss the effect of a properly described halo, let me first describe briefly a temporal sequence in the bar formation and evolution process.

Most N -body simulations start with a thin axisymmetric disc immersed in a more or less massive halo. The initial density and velocity distributions are chosen so as to be in agreement with observations of nearby spirals. Of course such initial conditions are idealised and may not hold for real galaxies, where the bar could well form at the same time as the disc. Yet, following the disc and bar formation *ab initio*, in a cosmological scenario, is a still largely unsolved problem, since it requires knowledge of the initial conditions of the mass distribution right after the formation of a disc galaxy. Furthermore, using present day initial conditions makes it possible to study best the angular momentum exchange and to make comparisons with analytical calculations. Nevertheless, problems like bar formation in a growing disc, non-spherical and/or clumpy haloes and the effect of infalling small satellites and debris need to be soon addressed.

Bar formation in such idealised initial conditions is illustrated in Fig. 1, which gives the face-on, the side-on and the edge-on views of the disc component at various times. I call side-on the edge-on view where the line-of-sight is along the bar minor axis, while the end-on view is also edge-on but with the line-of-sight along the bar major axis. At the beginning the disc starts axisymmetric, but soon forms spirals (not shown here), whose multiplicity depends on the disc-to-halo mass ratio within the outer disc radius. The actual bar formation time also depends on the relative importance of the halo component, being shorter in simulations whose inner parts are more disc dominated. In the second of the times illustrated the bar is still short and rather asymmetric. With time, it grows more symmetric, but also longer, i.e. stronger. At the last time shown, a ring structure encircles the bar. It is somewhat elongated, but not far from circular, as inner rings observed in barred galaxies (Buta, 1986). In all simulations the bar is direct, i.e. rotates in the same sense as the particles in the disc, and stops within corotation, in good agreement with periodic orbit calculations (Contopoulos, 1980).

Viewed edge-on, the disc shows also clear evolution. During the first stages of its formation, the bar stays thin, but thickens shortly

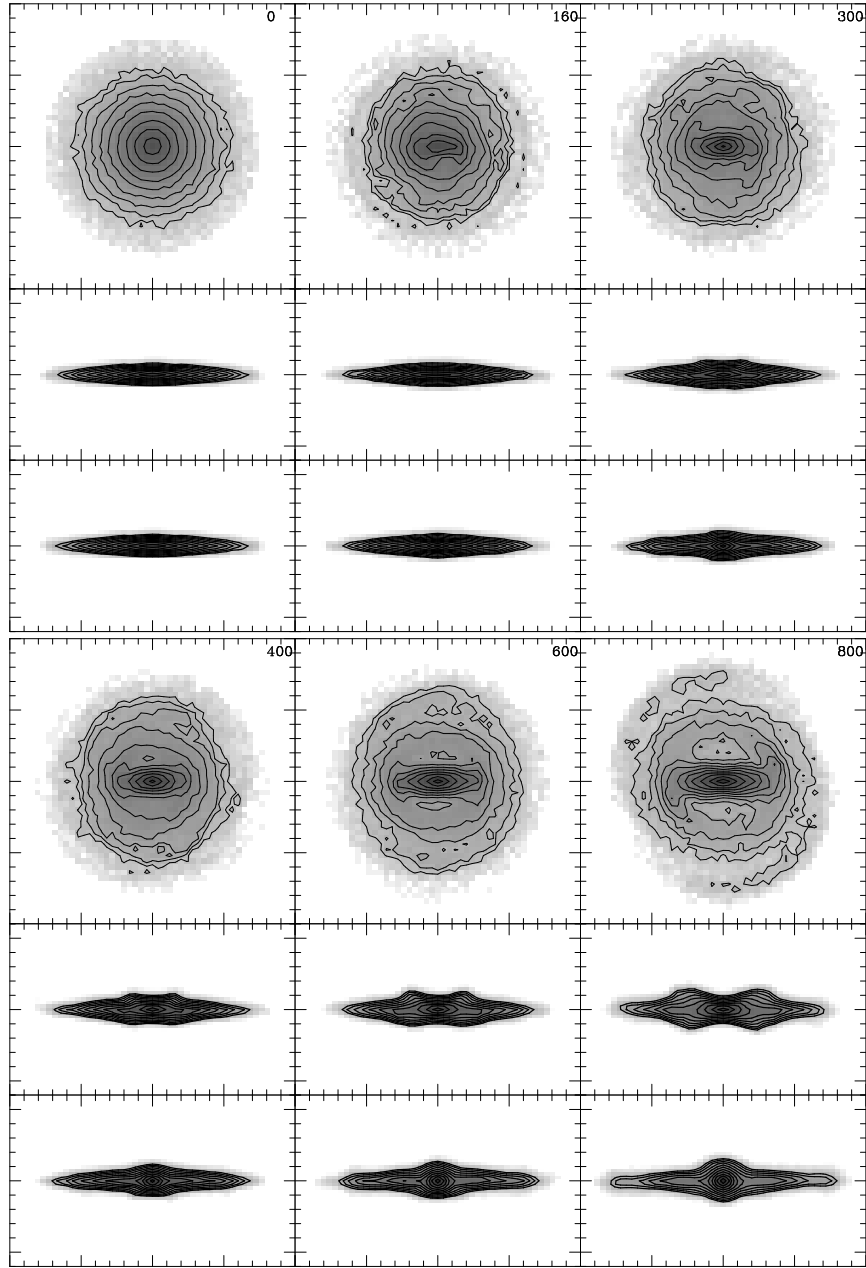


Figure 1. Formation of a bar in an initially axisymmetric disc. The upper and fourth rows give the face-on views; the second and fifth ones the side-on views and the third and sixth rows the end-on views. Time increases from left to right and from top to bottom and is given in the upper right corner of each face-on panel. Here and elsewhere in this paper, times are given in computer units as defined by Athanassoula and Misiriotis (2002).

thereafter. Its vertical extent increases as the bar strength increases. Initially its shape is boxy and then gradually evolves to peanut-like. Seen end-on the bar looks round, reminiscent of a bulge in the central part of a disc. Seen this way also, the bar size increases as it strengthens in the face-on view.

2. Angular momentum exchange

In a ground-breaking paper, Lynden-Bell and Kalnajs (1972) discuss the transport of angular momentum within discs of spiral galaxies. Using a full analytical treatment, as well as a simple but insightful individual orbit approach, they show that disc stars at inner Lindblad resonance (hereafter ILR) emit angular momentum, while disc stars at corotation (hereafter CR) and outer Lindblad resonance (hereafter OLR) absorb it, so that angular momentum is transported outwards. If the spiral amplitude is growing, material which is not at near-resonance can also emit, or absorb, angular momentum.

Athanassoula (2003a) extended the work of Lynden-Bell and Kalnajs to include a spheroidal component. If the distribution function of this component depends only on the energy, then all halo resonances will absorb angular momentum. Thus the picture of Lynden-Bell and Kalnajs can be generalised as follows : Angular momentum is emitted from material at near-resonance in the bar region (ILR and other such resonances within CR, e.g. 1:4; see Appendix for the notation) and absorbed by material at resonance in the outer disc and in the halo. Colder material can emit/absorb more angular momentum than hotter one. Thus the halo is less responsive than the disc per equal amount of resonant mass. However, there is not much material in the outer disc, where the density is very low, while the halo can be very massive. It can thus be that the halo absorbs more angular momentum than the outer disc, and this has proven to be the case in many N -body simulations, as will be discussed in the next section. Since the bar is a negative angular momentum ‘perturbation’ (Kalnajs 1971, Lynden-Bell and Kalnajs 1972), by losing angular momentum it becomes stronger.

Tremaine and Weinberg (1984) investigated dynamical friction on a solid bar rotating in a spherical halo and found that this arises from halo stars which are near-resonant with the rotating bar. They derived an analogue of Chandrasekhar’s formula (Chandrasekhar, 1943) for spherical systems, valid when the angular velocity of the bar does not change too slowly. Weinberg (1985) calculated that this will cause a considerable slow-down of the bar within a few bar rotations. As we will see in the next section, N -body simulations also present such a

slow down (e.g. Little and Carlberg 1991a, Little and Carlberg 1991b, Hernquist and Weinberg 1992, Athanassoula 1996, Debattista and Sellwood 2000, Valenzuela and Klypin 2003), but considerably less than that predicted by Weinberg (1985). Weinberg (2004) stressed that the derivation of the formulae of Lynden-Bell and Kalnajs assumes that the perturbations grow slowly over a very long time and that transients can be ignored. Their quantitative results should thus not be relied upon, since these assumptions may not hold in real galaxies. This, however, does not affect any of the results reviewed in this section, since they do not rely on any quantitative use of the Lynden-Bell and Kalnajs formalism.

Fuchs (2004) showed that the dynamics of a self-gravitating shearing sheet are strongly modified if this is immersed in a live halo. Namely, the amplitude of the density wave is very considerably enhanced. This work is presently being generalised to non-isotropic velocity distributions.

3. Results from N -body simulations

Contrary to real galaxies, N -body simulations are well suited for studying the angular momentum exchange within a galaxy. This has been one of the main goals of Athanassoula (2002) and Athanassoula (2003a) and I will retrace here a number of the steps made in those papers.

The first point to check is that there is a considerable amount of near-resonant material in the halo component. This is shown in the upper panels of Fig. 2, where I plot the mass per unit frequency ratio, M_R , as a function of the frequency ratio $(\Omega - \Omega_p)/\kappa$ (see appendix for the notation). It is clear that the distribution is not uniform, and has peaks at the resonances. In all simulations, the disc has a strong peak at ILR, which is made of particles trapped around this resonance and constituting the backbone of the bar. Secondary peaks can be found at other resonances, as e.g. inner 1:3, inner 1:4, CR or OLR, whose existence and height varies from one simulation to another. More important, the halo component also shows similar peaks. The highest is at CR, while secondary peaks can be seen at ILR and OLR. Such peaks can be seen in all simulations I analysed, again with varying heights.

The bottom panels of Fig. 2 show the way the angular momentum is exchanged. For the disc component it is emitted from the region within the bar, and particularly the ILR, and absorbed at CR (and in some simulations also at OLR). However, the amount of angular momentum emitted is much more than what the outer disc absorbs. This is understood with the help of the bottom right panel, which shows that all the halo resonances absorb a considerable amount of angular momentum,

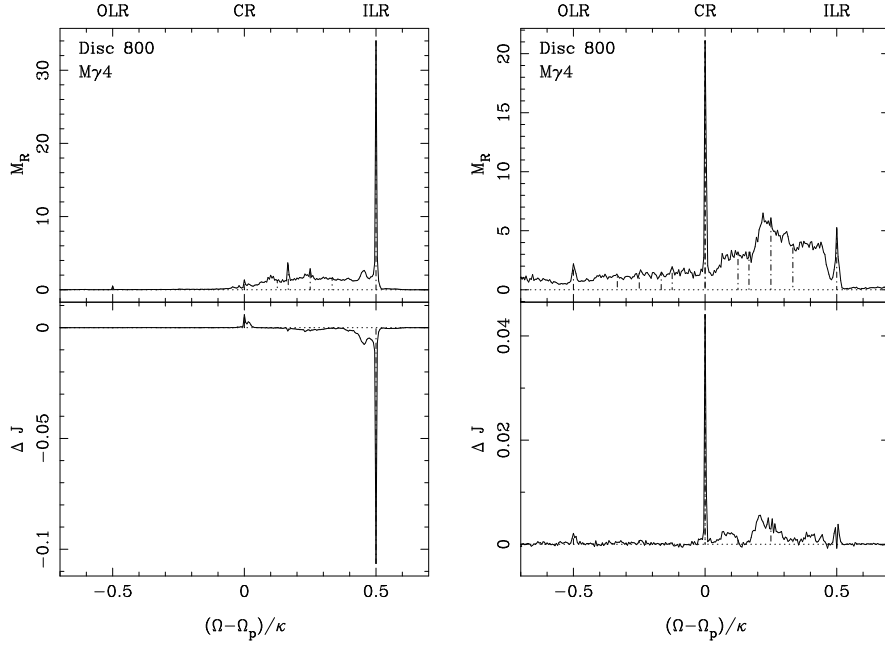


Figure 2. Resonances in the disc and the spheroidal component. The upper panels give, for the time $t = 800$, the mass per unit frequency ratio, M_R , as a function of that ratio. The frequency ratio is defined as $(\Omega - \Omega_p)/\kappa$, the ratio of the angular frequency in the frame in which the bar is at rest to the epicyclic frequency. The lower panels give ΔJ , the angular momentum gained or lost by particles of a given frequency ratio between times 500 and 800, as a function of that frequency ratio, calculated at $t = 800$. The left panels correspond to the disc component and the right ones to the spheroid. The vertical dot-dashed lines give the positions of the main resonances. The component and time are given in each panel. This figure is similar to figure 1 of Athanassoula (2003a), but now more particles have been used in the frequency calculations of the spheroidal component, so as to improve the signal to noise ratio. This is particularly clear in the lower right panel.

much more so than the outer disc. Thus simulations confirm the angular momentum exchange mechanism suggested by the analytical work, and show that the halo can be an important agent in this respect.

The global redistribution of angular momentum is seen in Fig. 3. This shows that the disc component loses a considerable amount of angular momentum which is taken by the halo. The amount of course varies from one simulation to another and depends on the parameters of the disc and the halo. Such a redistribution was also seen by Debattista and Sellwood (2000) and by Valenzuela and Klypin (2003).

Fig. 4 shows that the angular momentum redistribution can be very important for the bar evolution. It compares two simulations with initially identical disc components and with haloes having initially

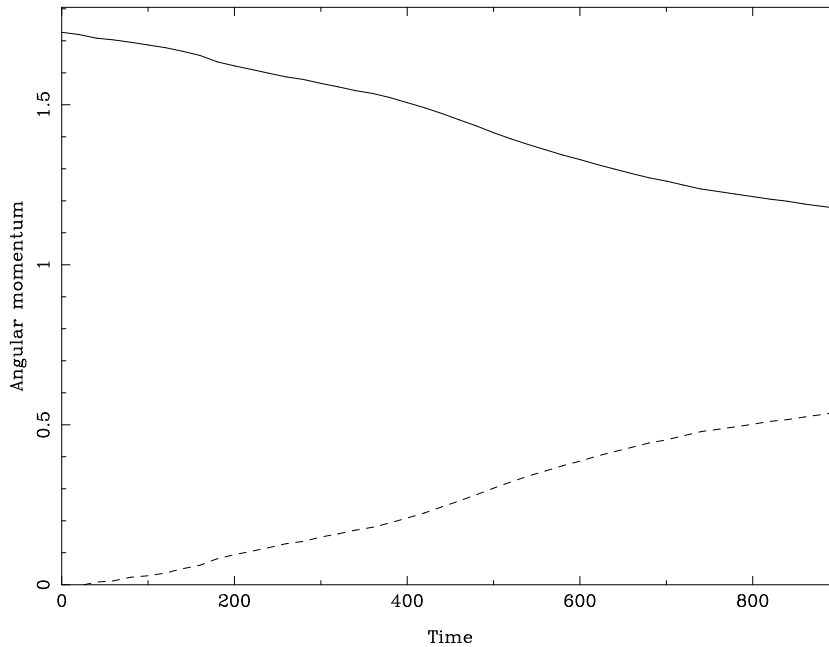


Figure 3. Angular momentum of the disc (full line) and spheroidal component (dashed line) as a function of time for a simulation producing a strong bar component.

identical mass distributions. In the simulation in the left panels the halo is live (LH), i.e. it is composed of particles. In the simulation in the right panels, however, the halo is rigid (RH), i.e. it is an imposed potential. Thus in LH the halo can absorb angular momentum, while in RH it can not. The difference in the evolution is very striking. Simulation LH grows a very strong bar, which, when seen side-on, has a strong peanut shape. Simulation RH, on the contrary, has a very mild oval in the innermost regions, and hardly evolves when seen edge-on. The large difference between the results of the two simulations argues strongly that the angular momentum absorbed by the halo can be a decisive factor in the evolution of the bar component.

Theoretical arguments predict that the angular momentum emitted or absorbed at a given resonance depends not only on the density of matter there, but also on how cold the near-resonant material is. This is borne out by the simulations. Indeed, if the disc is hot (i.e. has a high initial Q) and/or the halo is very hot, then the bar does not grow to be very strong and does not slow down much. Examples of this are given by Athanassoula (2003a).

In fact, it is the angular momentum redistribution that determines the strength and the slowdown rate of the bar. This can be seen in

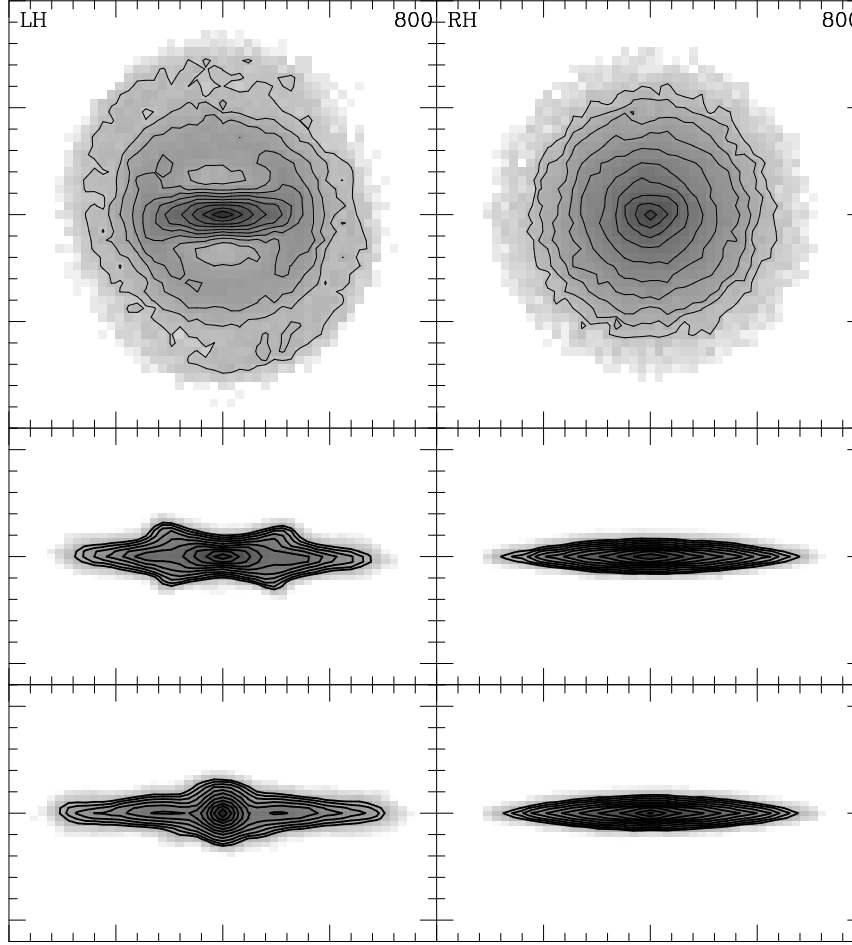


Figure 4. Comparison of two simulations with initially identical disc components and haloes with identical mass distributions. The time displayed is towards the end of the simulation. In the simulation displayed in the left panels the halo is live, i.e. it can respond to the disc evolution and exchange angular momentum with it. In the simulation in the right panels the halo is rigid, i.e. it is just a superposed constant potential, so that no angular momentum exchange between the disc and the halo is possible. The time is given in computer units in the upper right corner of the face-on views

Fig. 5, which includes results (i.e. strength and pattern speed of the bar and angular momentum absorbed by the halo) from a very large number of simulations, all with the same disc and halo masses and the same initial disc scale-length. The upper right panel shows that there is a clear correlation between the strength of the bar and the angular momentum absorbed by the halo component. The upper middle panel shows the corresponding relation, now for the bar pattern speed. Let

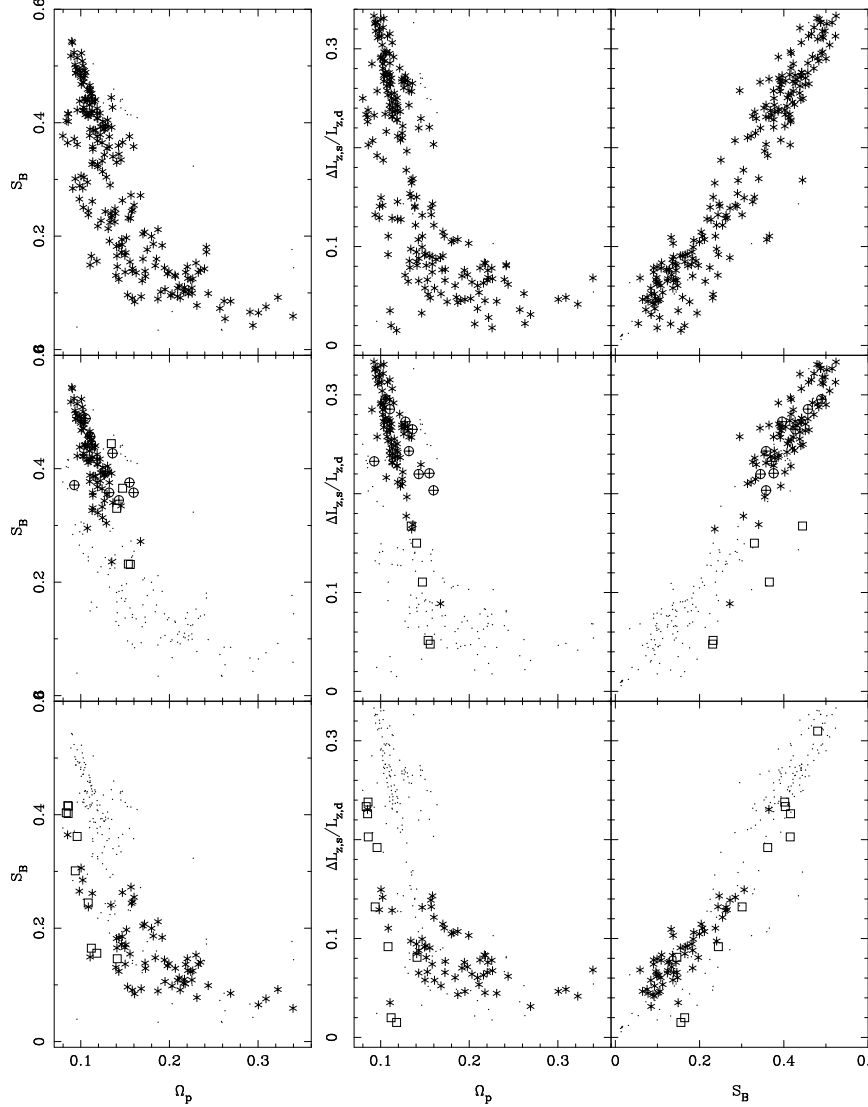


Figure 5. Relations between the bar strength and its pattern speed (left panels), the angular momentum acquired by the spheroid and the bar pattern speed (middle panels) and the angular momentum of the spheroid and the bar strength (right panels), at time $t = 800$. The spheroid angular momentum is normalised to the initial disc angular momentum ($L_{z,d}$). Each symbol represents the results of a simulation. The upper row includes all simulations. In the middle one, simulations with a concentrated halo (MH types in the notation of Athanassoula and Misiriotis 2002) are shown with a large symbol and those with a non-concentrated halo (MD types in the notation of Athanassoula and Misiriotis 2002) with a dot. MH simulations with a bulge are plotted with a circled cross, those with an initially very hot disc with an open square and the rest with a star. In the lower row simulations with a non-concentrated halo (MD types) are shown with a large symbol and those with a concentrated halo (MH types) with a dot. MD simulations with an initially very hot disc are singled out with an open square and the rest are given with a star.

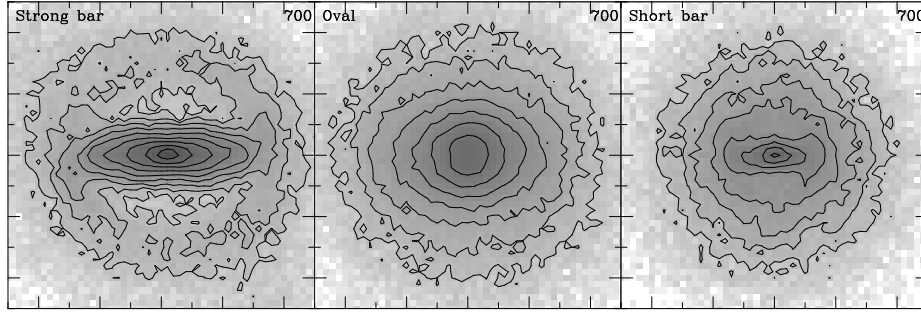


Figure 6. Three distinct bar morphologies. In the left panel the bar is strong, it has rectangular-like isodensities and is surrounded by a ring. In the middle panel the bar is an oval, while in the right panel it is short.

me now split the sample in two, one including simulations with haloes which have considerable mass in the regions of the main resonances, and one in which the halo mass is mainly in the parts outside the main resonances. In simulations in the first sample (middle row of panels), it is the halo that absorbs most of the angular momentum emitted by the bar region. A correlation between the pattern speed of the bar and the amount of angular momentum in the halo is thus expected, and is indeed found. In simulations in the second sample the disc plays a more important role in the angular momentum exchange, and only a weak trend with the angular momentum absorbed by the halo is expected, and this is indeed borne out by the simulations.

Such correlations are expected for all types of disc and spheroid models. The location of the regression line and of the individual points on the relevant planes – e.g. the $(\Delta L_{z,s}/L_{z,d}, S_B)$ plane, where $\Delta L_{z,s}$ the amount of angular momentum absorbed by the spheroid, $L_{z,d}$ the initial disc angular momentum, and S_B the bar strength – may well change with the model used.

The angular momentum exchange also determines the morphology of the bar. In all simulations where a considerable amount of angular momentum is redistributed, the bar is strong, as the example given in the left panel of Fig. 6. Such bars are long and have rectangular-like isodensities (Athanassoula and Misiriotis, 2002). They are often surrounded by a ring, whose location and shape is like those of the inner ring in real galaxies. The properties of such simulated bars are similar to those of strong bars in early type disc galaxies (Athanassoula, 2003b). This can be easily explained, since such galaxies have big bulges. These components are spheroids similar to the halo, and seen their extent, they will have near-resonant material which will absorb

angular momentum, thus helping the bar become yet stronger than it would in their absence.

Simulations in which little angular momentum has been exchanged do not form strong bars. Schematically, their morphology can be either that of an oval (middle panel of Fig. 6), or that of a short bar (right panel). Ovals are found predominantly in simulations with hot discs. Since in such cases it is the halo that absorbs most of the angular momentum, the bar can extend relatively far out in the disc to maximise the extent and therefore the contribution of the emitting region. Short bars are found predominantly in simulations with very hot, non-responsive haloes. Then the angular momentum absorbed by the outer disc is a considerable fraction of the total amount exchanged, and thus bars have to stay short in order to leave sufficient mass in the outer disc regions to do the absorption. Thus simulations can reproduce well the morphologies of observed bars and the wide range of bar strengths observed.

In Athanassoula (2003a) only the disc and halo (and sometimes bulge) components are taken into account. Yet the complete picture of angular momentum exchange can be more complicated. Galaxies (particularly late types) have also a gaseous disc component. This may give angular momentum to the bar, and thus decrease its strength (Berentzen et al., 2004). Furthermore, galaxies are not isolated universes, and thus can interact with their companions, or satellites. If the latter absorb angular momentum, then the bar can grow stronger than in the isolated disc (Berentzen et al., 2004). This is in good agreement with observational results that show that more bars can be found in interacting than in isolated galaxies (Elmegreen et al., 1990).

4. A bar in the halo component

Since the halo is not rigid, it evolves dynamically together with the disc. In simulations in which a considerable amount of angular momentum has been exchanged and which have thus formed a strong bar, the halo does not stay axisymmetric. It also forms a bar, or more precisely an oval, which I will call, for brevity, the halo bar. An example is seen in Fig. 7, which compares the morphology of the disc bar (upper panels) to that of the halo bar (lower panels). A very clear case of such a structure is also seen in Fig. 2 of Holley-Bockelmann et al. (2003).

Halo bars are triaxial, but nearer to prolate than to oblate, with their minor axis perpendicular to the disc equatorial plane. The axial ratio in this plane (ratio of minor to major axis) increases with increasing radius, so that halo bars tend to become axisymmetric in the outer

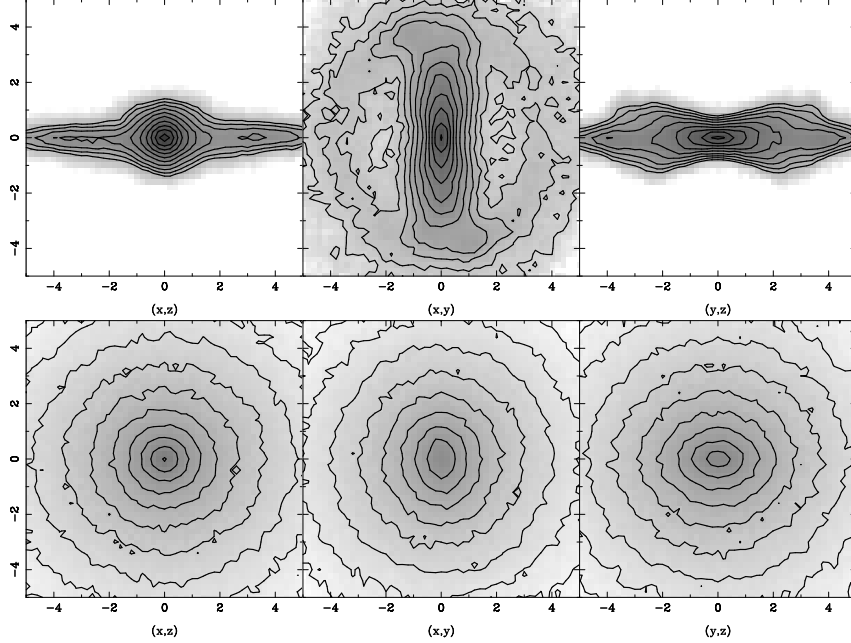


Figure 7. Three orthogonal views of the disc (upper panels) and halo components (lower panels). The central panel is a face-on view, while the two others are edge-on; side-on for the right panels and end-on for the left ones. Note that the halo component does not stay axisymmetric, but forms an oval in its inner parts, to which I refer to here as the halo bar.

parts. They are always considerably fatter than the corresponding disc bar, and thus nearer to ovals. Since the change in axial ratio is very gradual, it is not easy to define precisely the end of the halo bar, and thus to calculate its length. It is clear, however, that it is always considerably shorter than the disc bar. The length of the halo bar as a function of time for a simulation with a strong disc bar is given in Fig. 8. The spread in the measurements reflects the difficulty of defining precisely the end of the halo bar. Yet a least square fit shows clearly that the length of the halo bar increases with time. The slope of the dashed line gives the rate of increase of the disc bar length, and thus shows that the length of the halo bar increases less fast than that of the disc bar. The halo bar has roughly the same orientation as the disc bar at all times. In good agreement with Holley-Bockelmann et al. (2003), I find that the $m=2$ component of the halo continues also outside the halo bar, trailing behind the disc bar. More information on the halo bar properties, their relation with the disc bar properties, and the changes in the halo orbital structure as a result of the halo bar formation will be given elsewhere (Athanassoula, 2004b).

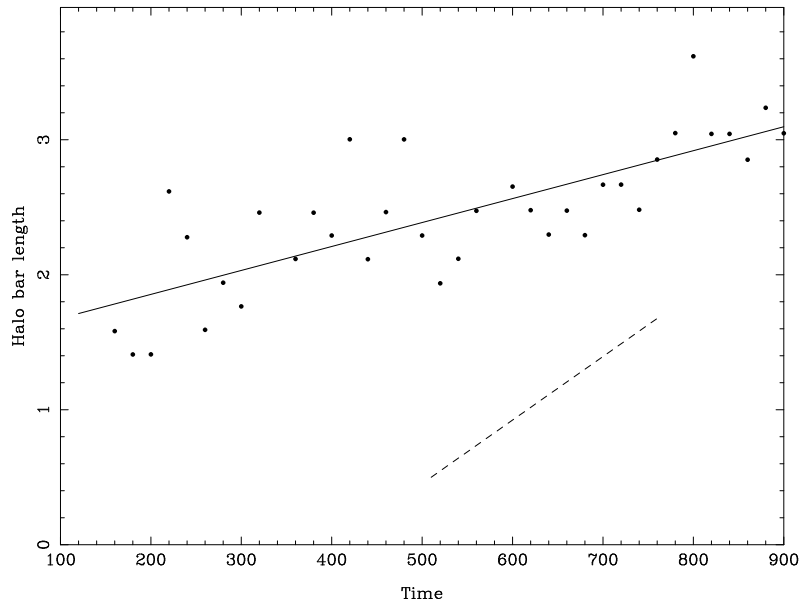


Figure 8. Length of the halo bar as a function of time. The solid line is a least square fit. The slope of the dashed line gives the growth of the length of the disc bar with time.

5. The formation of boxy/peanut features

N -body simulations show that bars form initially in the disc equatorial plane. Very shortly thereafter, however, they buckle out of this plane, creating initially an asymmetric structure which soon evolves into a symmetric peanut (Combes and Sanders 1981, Combes et al. 1990, Raha et al. 1991, Athanassoula and Misiriotis 2002, Athanassoula 2003a, O'Neill and Dubinski 2003, Athanassoula 2004a) The formation of such a structure is easily understood in the framework of orbital structure in 3D barred galaxy potentials. Such a study was initiated by Pfenniger (1984), who showed that there are several families of 3D orbits, bifurcated at the vertical resonances of the main planar family. This work was supplemented and extended in a series of four papers (Skokos et al. 2002a, 2002b, Patsis et al. 2002, 2003, also Patsis, 2002). I will briefly recall here the main results of these papers that are relevant to the formation of the peanut structure. I will also follow their notation.

2D orbital structure studies clearly established that it is the stable members of the x_1 family of periodic orbits (i.e. the orbits that are elongated along the bar and close after one rotation and two radial

oscillations) that constitute the backbone of the bar (Contopoulos and Papayannopoulos 1980, Athanassoula et al. 1983, etc.). Such periodic orbits trap around them regular, non-periodic orbits and, due to their appropriate size, shape and orientation, form the bar.

3D orbital studies, however, showed that the situation is much more complicated. The backbone of 3D bars is the x_1 tree, i.e. the x_1 family plus a tree of 2D and 3D families bifurcating from it (Skokos et al. 2002a, Skokos et al. 2002b). Trapping around these families will determine the extent and shape of the bar in the face-on view, as well as the edge-on extent and shape. However, it need not be the same family that determines both. The radial extent and outer outline in the face-on view is usually determined by the x_1 family and/or 2D rectangular-like orbits at the planar 4:1 resonance region. On the other hand, the length of the peanut is determined by the extent of the 3D family that constitutes its backbone, e.g. the x_{1v1} , or the x_{1v4} family (see Skokos et al. 2002a for more information on these families and their properties). This means that the length of the peanut must be somewhat shorter than that of the bar seen face-on, the exact ratio depending on which family(ies) constitute(s) the backbone of the peanut. It is important to note that the (x,y) projection of the members of the families of the x_1 tree has, in general, an outline which is very similar to that of the members of the x_1 family (2D orbits) at the same energy. This means that the difference between the two stands out in the edge-on view, but can be seen only little in the face-on view.

The vertical family which bifurcates from the x_1 at the lowest energy – x_{1v1} in the notation of Skokos et al. (2002a) – is particularly useful for building boxy or peanut-like features if it does not have a sizeable complex unstable part. If this family is the backbone of the peanut, then this feature is considerably shorter than the bar, the ratio of the two being less than 0.5 in the models of Patsis et al. (2002). On the other hand, if the backbone is a family which bifurcates at higher energies, then the peanut/bar ratio is considerably larger. E.g. if the backbone is the x_{1v4} family, then the ratio is of order of 0.8. In this case the vertical extension of the peanut or boxy feature is also considerably less. If more than one vertical family contributes significantly to the peanut, it is generally the one which bifurcates at the lowest energy that plays the main role morphologically. Finally, it is worth mentioning that 3D families which bifurcate from the x_2 family (i.e. from the planar family which is elongated perpendicular to the bar) can also support boxy morphologies. This can influence the morphology of bars seen end-on.

Such boxy or peanut structures, when seen in real galaxies, are called by observers “boxy or peanut bulges”. This is due to the fact that, according to the simple morphological definition, a bulge is a smooth

light distribution that swells out of the central part of the disc seen edge-on; a definition that is well fulfilled by boxy/peanut structures. However, bulges are not a homogeneous class of objects. As discussed by Athanassoula (2004a), they include classical bulges, boxy/peanut features, and disc-like bulges. Classical bulges have spheroidal shapes, a maximum thickness (seen edge-on) at the center of the galaxy, and a projected light, or surface density, profile close to the $r^{\frac{1}{4}}$ law. They presumably form from hierarchical merging and/or collapse. On the other hand, boxy/peanut features are just part of the bar. In fact, as already discussed, they are the part that is composed of the vertically extending orbits from 3D families which bifurcate from the x_1 family. Finally, disc-like bulges are central disc-like objects formed from gaseous material pushed inwards by torques due to bars, or perhaps other non-axisymmetric features, which later formed stars. This last class of objects has been mainly defined with the help of radial photometric profiles, i.e. they are excess light in the central part of disc galaxies, above the simple exponential profile fitting the remaining, non-central part of the disc.

Athanassoula (2004a) presented a number of comparisons of observed properties of boxy/peanut features with those of edge-on bars and found excellent agreement. I will here discuss two such comparisons, namely the comparison of the features in median filtered images, and the features in the emission line and absorption line position – velocity diagrams, and refer the reader to Athanassoula (2004a) for others.

5.1. MEDIAN FILTERING

A comparison of images of real galaxies and of simulated ones after comparable median filtering is much more demanding than a comparison of the corresponding global morphologies. This is due to the fact that median filtering reveals a number of features, whose position and form have to be matched at a given scale.

Aronica et al. (2003, 2004) have performed median filtering of near-infrared images of a sample of edge-on boxy and peanut galaxies and found a number of interesting features. In many cases (e.g. Fig. 2a in Aronica et al., 2003) one can note four extensions out of the equatorial plane, which form an X-like shape, except that the four extensions do not necessarily cross the center. Another common feature is maxima of the density along the equatorial plane, away from the center and diametrically opposite. Namely, starting from the center of the galaxy and going outwards along the equatorial plane, the projected surface

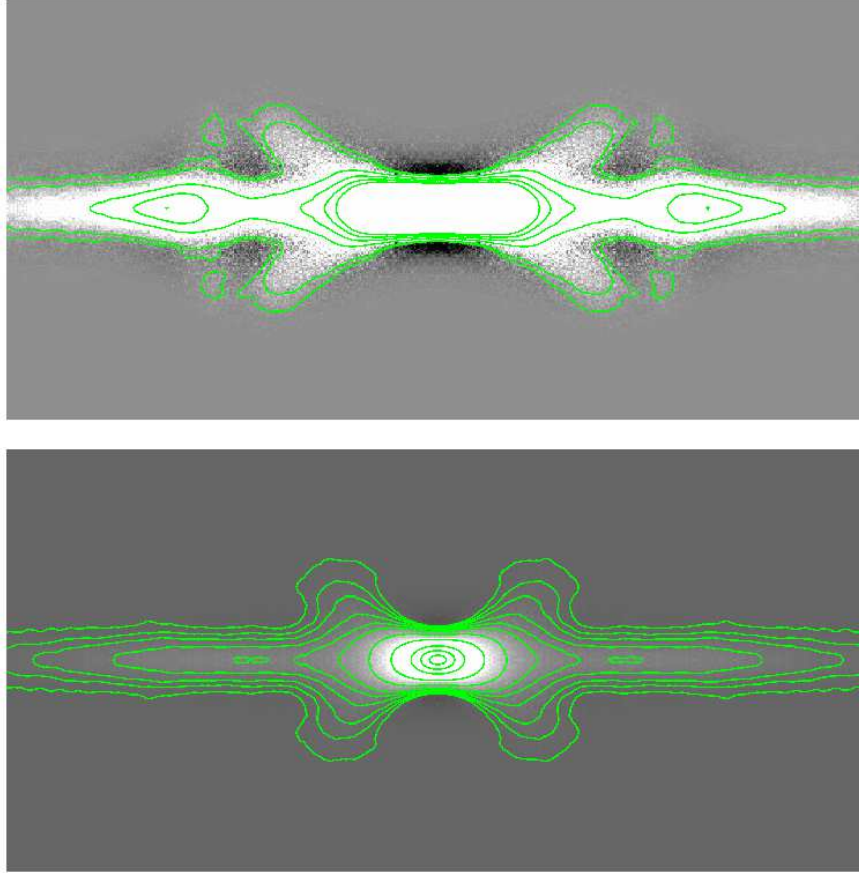


Figure 9. Median filtered image for the disc of a simulation with a strong bar. In the upper panel the bar is seen side-on, and in the lower panel it is seen edge-on with the line-of-sight at 45° to the bar major axis. The isodensities are chosen so as to show best the relevant features.

density first drops and then increases again to reach a local maximum. It then decreases to the edge of the disc.

In order to compare the simulations to the observations, I applied to the former a similar analysis, using the same software. The full procedure is described in Athanassoula (2004a). The results for two different viewing angles are shown in Fig. 9 for a simulation with a strong bar. The similarity between the features in the median filtered observations and simulations is very striking.

In the upper panel of Fig. 9 the disc is viewed edge-on, with the bar side-on. It displays a clear X-like form, and secondary maxima on the equatorial plane on either side of the center, in good agreement with median filtered images of observed galaxies with peanuts. It further

shows two very faint features, like parentheses enclosing the X. The lower panel of Fig. 9 shows the same simulation but from a viewing angle of 45° . Viewed side-on, the four branches of the X do not cross the center. This is probably still true, but less easy to see, when the viewing angle is 45° . Furthermore, the outermost isodensity contours joining the two upper (or lower) branches of the X look curved. This can also be seen in a number of the median filtered galaxy images in Aronica et al. (2004), which might mean that these galaxies are seen from a viewing angle around 45° . Finally, the secondary maxima along the equatorial plane can be seen from both viewing angles (as well as from an end-on view not shown here), but are most prominent in the side-on view. All these features were seen in the median filtered images of the galaxies in Aronica et al. (2004). They are not accidental; they correspond to specific structures of the periodic orbits that constitute the backbone of barred galaxies (Patsis et al., 2002). A more thorough comparison of the observations, the simulations and the periodic orbit structure will be given elsewhere (see also Aronica et al., 2004).

5.2. PVD DIAGRAMS

Emission line spectroscopy of boxy/peanut galaxies (Kuijken and Merrifield 1995, Merrifield and Kuijken 1999, Bureau and Freeman 1999) showed that their major axis position velocity diagrams (hereafter PVDs) show a number of interesting features which were first linked to bars by Kuijken and Merrifield. Bureau and Athanassoula (1999) used periodic orbits in a standard barred galaxy potential as a first step in understanding such features. Although this approach is too crude to reproduce, even roughly, observed PVDs, it can still give useful insight. For example, it showed that the superposition of the main periodic orbit families leads to gaps between the signatures of the different orbit families, as well as to material in the so-called forbidden quadrants. To actually model emission line PVDs, Athanassoula and Bureau (1999) used the gas flow simulations of Athanassoula (1992) viewed edge-on. They found that shocks along the leading edges of the bar and the corresponding inflow lead to a characteristic gap in the PVDs, between the signature of the nuclear spiral (whenever existent) and the signature of the disc. There is in general very good agreement between the signatures of the observed emission line PVDs and those obtained by hydrodynamic models.

Chung and Bureau (2004) presented long-slit absorption line kinematic observations of 30 edge-on disc galaxies, most of which have a boxy structure or a peanut. They analysed the corresponding PVDs using Gauss-Hermite series and produced profiles of the integrated light

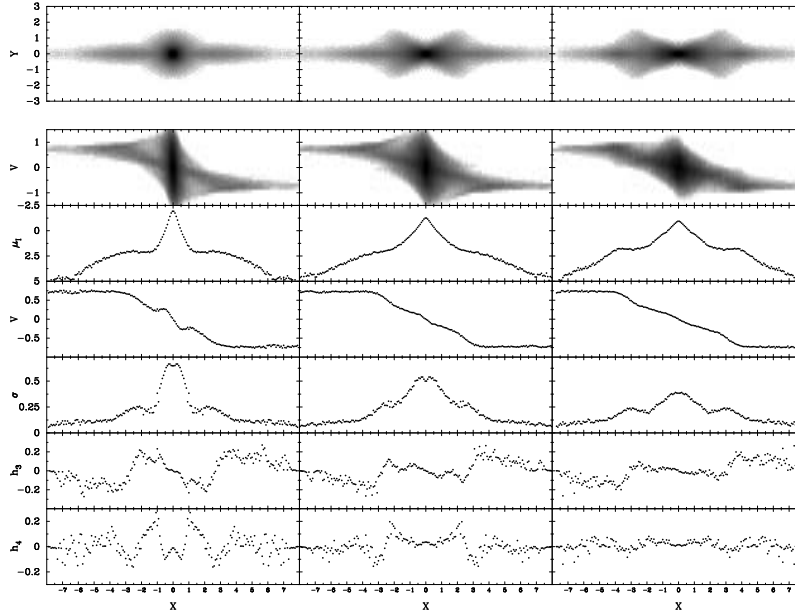


Figure 10. Analysis of the kinematic information obtained along the equatorial plane of an edge-on N -body disc galaxy with a strong bar. The three columns correspond to different viewing angles. In all three the disc is seen edge-on. In the left panels the bar is seen end-on, in the right panels side-on, and in the central ones the line-of-sight is oriented at 45° with respect to the bar major axis. The upper row gives a greyscale representation of the disc material. The second row gives the corresponding position - velocity diagram, again in greyscale. The third row gives the surface brightness as function of distance along the equatorial plane. The fourth, fifth, sixth, and seventh rows give the velocity, σ , h_3 and h_4 , respectively, where σ is the velocity dispersion, and h_3 and h_4 are the 3rd and 4th components of the Gauss-Hermite series.

along the slit, the mean stellar velocity V , the velocity dispersion σ , as well as the higher order components h_3 and h_4 . Bureau and Athanassoula (2004) ‘observed’ many N -body bars seen edge-on, using for their analysis exactly the same techniques and, whenever possible, also the same software. It is thus both straightforward and meaningful to make comparisons of the results of the two studies.

The similarities are striking. Both studies find the same characteristic signatures, one in the observations and the other in the simulations. Fig. 10 gives the results for an N -body simulation with a strong bar. The integrated light along the slit (equivalent to a major-axis light profile) has a quasi-exponential central component and a plateau at intermediate radii, followed by a steep drop. The rotation curve shows a double hump. The velocity dispersion has a central peak, which in the center-most part may be rather flat or may even have a central minimum. At intermediate radii there can be a plateau which some-

times ends on either side with a shallow maximum before dropping steeply at larger radii. In fact, these features can already be seen in Figure 13 of Athanassoula and Misiriotis (2002), although the display adopted in that paper makes it more difficult to compare directly to observations. Fig. 10 also shows that h_3 correlates with V over most of the bar length, contrary to what is expected for a fast rotating disc. All these features are spatially correlated and are seen, more or less strongly, both in the observations and in the simulations. The N -body simulations show clearly that the strength of these features depends on the strength of the bar as well as on its viewing angle. Furthermore, those features can be interpreted with the help of the orbital structure in barred discs (Bureau and Athanassoula, 1999).

The only observed feature not found by Bureau and Athanassoula (2004) is the anti-correlation of h_3 and V in the center-most parts. Indeed, the observations show that, in a small region very near the center, the h_3 and V curves anti-correlate in many cases, while for the remaining bar region they correlate. On the hand, in the simulations shown by Bureau and Athanassoula (2004) the h_3 and V curves always correlate all the way to the center. This small discrepancy can be remedied in two ways, presented and discussed elsewhere (Athanassoula, in preparation). The first relies on the existence of a gaseous inner disc, present in the galaxies but not in the simulations discussed by Bureau and Athanassoula (2004), while the second relies on a more centrally concentrated halo profile. Thus even this small discrepancy between observations and simulations can be remedied.

6. Summary and discussion

Bars are present in the majority of observed disc galaxies and also form spontaneously in N -body simulations. Contrary to previous beliefs, it is now well established that haloes can destabilise bars, since they can take positive angular momentum from them and thus make them stronger and slower rotating. This of course will work only if all components are non-rigid and capable of emitting/absorbing angular momentum.

It is possible to account for the considerable spread in observed bar morphologies. These can range from short bars or ovals, which should be found in disc galaxies within which not much angular momentum has been exchanged, to very strong bars with rectangular-like isophotes, which on the contrary should be in galaxies having undergone considerable amount of angular momentum redistribution. Extreme cases of such galaxies are some examples of bar dominated early type discs

presented by Gadotti and de Souza (2003), in which the disc is not a major component any more, since a very considerable fraction of its mass is now within the bar component. Indeed, it is possible to turn the problem around and to try and obtain some information on galaxy haloes from the morphology of their bars. Even though no strong conclusions can be reached in this way, the insight thus obtained is still very welcome, since our knowledge on disc galaxy haloes is still very restricted. Thus short bars, like in our own Galaxy, should be indicative of very hot haloes, which could not absorb much angular momentum. On the contrary, strong and long bars, should be indicative of haloes that can absorb angular momentum, with considerable amount of material in the relatively inner regions where the resonances lie.

A short while after having formed, the bar buckles perpendicular to the disc equatorial plane and forms an edge-on boxy or peanut shape. Detailed comparison of N -body bars with structures known as ‘boxy or peanut bulges’ – including morphology, photometry and kinematics – show that these so-called bulges are in fact the part of the bar sticking out of the equatorial plane of the galaxy. This behaviour and structure is easily understood with the help of the orbital structure in 3D barred galaxy potentials.

Appendix

In this appendix I summarise some elementary notions for orbits and resonances in order to introduce the notation and nomenclature used in this paper.

In galactic discs, many stars are on orbits which are not too far from circular, so that the epicyclic approximation is valid. Orbits on the equatorial plane of a disc galaxy are then characterised by two frequencies : the angular frequency Ω and the frequency of the radial motion, called epicyclic frequency, κ . In a frame of reference in which the bar (or, more generally, the non-axisymmetric perturbation) is at rest, the angular frequency becomes $\Omega - \Omega_p$, where Ω_p is the pattern speed. Resonances occur when the angular and radial frequencies are commensurable, i.e. when

$$\frac{\Omega - \Omega_p}{\kappa} = -\frac{l}{m}, \quad (1)$$

where l and m are integers, so that the orbit closes in the rotating frame of reference. If the orbit closes after one rotation and two radial oscillations, i.e. when $l = -1$ and $m = 2$, it is at inner Lindblad resonance (ILR). An example of such an orbit is shown in the middle

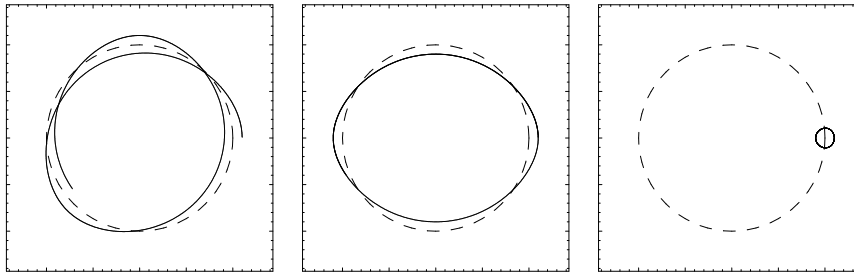


Figure 11. Three examples of epicyclic orbits. In the middle panel we have $l = -1$ and $m = 2$, so that the orbit is at the ILR. In the right panel we have $l = 0$, so that the orbit is at corotation. In the left panel the l and m values are not commensurable, so that the orbit does not close.

panel of Fig. 11. For $l = 1$ and $m = 2$ the orbit is at the outer Lindblad resonance (OLR). If the orbit is at corotation (CR), then $l = 0$ (right panel of Fig. 11). Further resonances of importance to bars are the inner ultra-harmonic resonance (iUHR) with $l = -1$ and $m = 4$, and in general all resonances with $l = -1$. If the l and m values are not commensurable the orbit will not close (left panel of Fig. 11). Epicyclic orbits in three dimensions have one more frequency, the frequency of the vertical oscillation (κ_z), so that further resonances are possible. For example if

$$\frac{\Omega - \Omega_p}{\kappa_z} = -\frac{n}{m} \quad (2)$$

with $n = -1$ and $m = 2$, then the orbit is at the vertical ILR, often named the 2:1 vertical resonance. Vertical resonances of the $m:1$ type are in general important since they can introduce families which are crucial for building the peanut structure.

Of course, in general orbits are not simple epicycles, yet working in action-angle variables (e.g. Binney and Tremaine, 1987) makes it possible to deal with the regular orbits in ways similar to those used for epicycles, and in particular to define resonances in a similar way. It is also possible to determine the principal frequencies of an orbit numerically (Binney and Spergel, 1982) and this can be made even for potentials which are not known in a closed analytical form, as e.g. those from N -body simulations.

Acknowledgements

In the past four years, during which I was working on the subject matters discussed in this paper, I benefitted from a number of interesting

and motivating discussions with A. Bosma, M. Bureau, W. Dehnen, A. Misiriotis, P. Patsis, M. Tagger, G. Aronica, I. Berentzen, K. Freeman, B. Fuchs, A. Kalnajs, J. Kormendy, D. Lynden-Bell, F. Masset, and Ch. Skokos. I thank Jean-Charles Lambert for his invaluable help with the simulation software and the administration of the runs and W. Dehnen for making available to me his tree code and related programs. I also thank the Observatoire de Marseille, the region PACA, the INSU/CNRS and the University of Aix-Marseille I for funds to develop the computing facilities used for the calculations in this paper.

References

- Aronica, G., E. Athanassoula, M. Bureau, A. Bosma, R.-J. Dettmar, D. Vergani and M. Pohlen. Comparing peanut shaped “bulges” to N -body simulations and orbital calculations. *Astrophysics and Space Science*, 284:753–756, 2003.
- Aronica, G., M. Bureau, E. Athanassoula, A. Bosma, R.-J. Dettmar and K.C. Freeman. K-band observations of boxy bulges. I. Morphology and major-axis surface brightness profiles. *In preparation*, 2004.
- Athanassoula, E. The existence and shapes of dust lanes in galactic bars. *Monthly Notices of the Royal Astronomical Society*, 259:345–364, 1992.
- Athanassoula, E. Evolution of bars in isolated and interacting disk galaxies. In R. Buta, D.A. Crocker and B.G. Elmegreen *Barred Galaxies*, pages 309–321, Astron. Soc. Pac. Conf. Series 91, 1996.
- Athanassoula, E. Bar-halo interaction and bar growth. *Astrophysical Journal Letters*, 569:L83–L86, 2003.
- Athanassoula, E. What determines the strength and the slowdown rate of bars? *Monthly Notices of the Royal Astronomical Society*, 341:1179–1198, 2003a.
- Athanassoula, E. Isolated and interacting galaxies : simulations with GRAPE. In J. Makino and P. Hut, editors, *Astrophysical supercomputing using particles*, Astron. Soc. Pac. Conference Series, IAU Symp. 208, 208:177–188, 2003b.
- Athanassoula, E. On the nature of bulges in general and box/peanut ‘bulges’ in particular. Input from N -body simulations. *Monthly Notices of the Royal Astronomical Society*, submitted, 2004a.
- Athanassoula, E. Existence and properties of a bar in the inner halo of barred galaxies. *in preparation*, 2004b.
- Athanassoula, E., O. Bienaymé, L. Martinet and D. Pfenniger. Orbits as building blocks of a barred galaxy model. *Astronomy and Astrophysics* 127:349–360, 1983.
- Athanassoula, E. and M. Bureau. Bar diagnostics in edge-on spiral galaxies. II. Hydrodynamical simulations. *Astrophysical Journal*, 552:699–717, 1999.
- Athanassoula, E. and A. Misiriotis. Morphology, photometry and kinematics of N body bars. I Three models with different halo central concentrations. *Monthly Notices of the Royal Astronomical Society*, 330:35–52, 2002.
- Athanassoula, E. and J. A. Sellwood. Bi-symmetric instabilities of the Kuz'min/Toomre disc. *Monthly Notices of the Royal Astronomical Society*, 221:213–232, 1986.
- Berentzen, I., E. Athanassoula, C. H. Heller and K. J. Fricke. The regeneration of stellar bars by tidal interactions. Numerical simulations of fly-by encounters. *Monthly Notices of the Royal Astronomical Society*, 347:220–236, 2004.

- Binney J. and D. Spergel. Spectral stellar dynamics. *The Astrophysical Journal*, 252:308–321, 1982.
- Binney J. and S. Tremaine. Galactic Dynamics. Princeton Univ. Press, 1987.
- Bureau, M. and E. Athanassoula. Bar Diagnostics in Edge-on Spiral Galaxies. I. The Periodic Orbits Approach. *The Astrophysical Journal*, 552:686–698, 1999.
- Bureau, M. and E. Athanassoula. Bar Diagnostics in Edge-on Spiral Galaxies. III. N -body simulations of disks. *The Astrophysical Journal*, submitted, 2004.
- Bureau, M. and K.C. Freeman. The Nature of Boxy/Peanut-Shaped Bulges in Spiral Galaxies. *Astronomical Journal*, 118:126–138, 1999.
- Buta, R.J. The structure and dynamics of ringed galaxies I. The morphology of galaxy rings and statistics of their apparent shapes and apparent orientations with respect to bars. *Astrophysical Journal Supplements*, 61:609–630, 1986.
- Chandrasekhar, S. Dynamical friction. I. General considerations: the coefficient of dynamical friction. *Astrophysical Journal*, 97:255–262, 1943.
- Chung, A. and M. Bureau. Stellar kinematics of boxy bulges : Large-scale bars and inner disks. *Astronomical Journal*, 127:3192–3212, 2004.
- Combes, F. and R.H. Sanders. Formation and properties of persisting stellar bars. *Astronomy and Astrophysics*, 96:164–173, 1981.
- Combes, F., F. Debbasch, D. Friedli and D. Pfenniger. Box and peanut shapes generated by stellar bars. *Astronomy and Astrophysics*, 233:82–95, 1990.
- Contopoulos G. How far do bars extend. *Astronomy and Astrophysics*, 81:198–209, 1980.
- Contopoulos G. and T. Papayannopoulos. Orbits in weak and strong bars. *Astronomy and Astrophysics*, 92:33–46, 1980.
- Debattista, V. P. and J. A. Sellwood. Constraints on dynamical friction on the dark matter content of barred galaxies. *Astrophysical Journal*, 543:704–721, 2000.
- Elmegreen, D.M., B.G. Elmegreen and A.D. Bellin. Statitital evidence that galaxy companions trigger bars and change Hubble types. *Astrophysical Journal*, 364:415–419, 1990.
- Eskridge et al. The frequency of barred spirals in the near-infrared. *Astronomical Journal*, 119:536–544, 2000.
- Fuchs, B. Density waves in the shearing sheet. IV Interaction with a live dark halo.. *Astronomy and Astrophysics*, 419:941–948, 2004.
- Gadotti, D. A. and R. E. de Souza NGC 4608 and NGC 5701: barred galaxies without disks ? *Astrophysical Journal*, 583:L75–L78, 2003.
- Grosbøl P., E. Pompei, and P.A. Patsis. Spiral structure observed in the near-infrared. In E. Athanassoula, A. Bosma and R. Mujica *Disks of galaxies : Kinematics, dynamics and perturbations*, pages 305–310, Astron. Soc. Pac. Conf. Series 275, 2002.
- Hernquist, L. and M. Weinberg. Bar-spheroid interaction in galaxies. *Astrophysical Journal*, 400:80–95, 1992.
- Hohl, F. Numerical experiments with a disc of stars *Astrophysical Journal*, 168:343–359, 1971.
- Holley-Bockelmann, K., M. D. Weinberg, and N. Katz. Bar-induced evolution of dark matter cusps. *astro-ph/0306374*, 2003.
- Kalnajs, A. J. Dynamics of flat galaxies I *Astrophysical Journal*, 166:275–293, 1971.
- Kuijken K. and M. R. Merrifield. Establishing the connection between peanut shaped bulges and galactic bars. *Astrophysical Journal*, 443:L13–L16, 1995.
- Little, B. and R. G. Carlberg. The long-term evolution of barred galaxies. *MNRAS*, 250:161–170, 1991a.

- Little, B. and R. G. Carlberg. Bar-disc angular momentum exchange. *MNRAS*, 251:227–242, 1991b.
- Lynden-Bell, D. and A. J. Kalnajs. On the generating mechanism of spiral structure. *Monthly Notices of the Royal Astronomical Society*, 157:1–30, 1972.
- Merrifield, M. R. and K. Kuijken. Hidden bars and boxy bulges. *Astronomy and Astrophysics*, 345:L47–L50, 1999.
- Miller, R. H., K. H. Prendergast and W. J. Quirk. Numerical experiments on spiral structure. *Astrophysical Journal*, 161:903–916, 1970.
- O’Neill, J. K. and J. Dubinski. Detailed comparison of the structures and kinematics of simulated and observed barred galaxies. *Monthly Notices of the Royal Astronomical Society*, 346:251–264, 2003.
- Ostriker, J. P. and P. J. E. Peebles. A numerical study of the stability of flattened galaxies : or can cold galaxies survive? *Astrophysical Journal*, 186:467–480, 1973.
- Patsis, P.A. Orbital morphology of 3D bars. In E. Athanassoula, A. Bosma and R. Mújica *Disks of galaxies : Kinematics, dynamics and perturbations*, pages 161–168, Astron. Soc. Pac. Conf. Series 275, 2002.
- Patsis, P.A., Ch. Skokos and E. Athanassoula. Orbital dynamics of three dimensional bars - III Boxy/peanut edge-on profiles. *Monthly Notices of the Royal Astronomical Society*, 337:578–596, 2002.
- Patsis, P.A., Ch. Skokos and E. Athanassoula. Orbital dynamics of three dimensional bars - IV Boxy isophotes in face-on views. *Monthly Notices of the Royal Astronomical Society*, 342:69–78, 2003.
- Pfenniger, D. The 3D dynamics of barred galaxies. *Astronomy and Astrophysics*, 134:373–386, 1984.
- Raha, N., J. A. Sellwood, R. A. James and F. D. Kahn. A dynamical instability of bars in disk galaxies. *Nature*, 352:411–412, 1991.
- Skokos, Ch., P.A. Patsis and E. Athanassoula. Orbital dynamics of three dimensional bars - I The backbone of three dimensional bars. A fiducial case. *Monthly Notices of the Royal Astronomical Society*, 333:847–860, 2002.
- Skokos, Ch., P.A. Patsis and E. Athanassoula. Orbital dynamics of three dimensional bars - II Investigation of the parameter space. *Monthly Notices of the Royal Astronomical Society*, 333:861–870, 2002.
- Tremaine, S. and M. Weinberg. Dynamical friction in spherical systems. *Monthly Notices of the Royal Astronomical Society*, 209:729–757, 1984.
- Valenzuela, O. and A. Klypin. Secular bar formation in galaxies with significant amount of dark matter. *Monthly Notices of the Royal Astronomical Society*, 345:406–422, 2003.
- Weinberg, M. Evolution of barred galaxies by dynamical friction. *Monthly Notices of the Royal Astronomical Society*, 213:451–471, 1985.
- Weinberg, M. Time-dependent secular evolution in galaxies. *Monthly Notices of the Royal Astronomical Society*, astro-ph/0404169, 2004.